CrossMark

Interpreting the Strongly Lensed Supernova iPTF16geu: Time Delay Predictions, Microlensing, and Lensing Rates

Anupreeta More[1], Sherry H. Suyu[2,3,4], Masamune Oguri[1,5,6], Surhud More[1], and Chien-Hsiu Lee[7]

[1] Kavli Institute for the Physics and Mathematics of the Universe (Kavli IPMU, WPI), University of Tokyo, Chiba 277-8583, Japan; anupreeta.more@ipmu.jp
[2] Max-Planck-Institut für Astrophysik, Karl-Schwarzschild-Str. 1, D-85748 Garching, Germany
[3] Institute of Astronomy and Astrophysics, Academia Sinica, P.O. Box 23-141, Taipei 10617, Taiwan
[4] Physik-Department, Technische Universität München, James-Franck-Straße 1, D-85748 Garching, Germany
[5] Department of Physics, University of Tokyo, 7-3-1 Hongo, Bunkyo-ku, Tokyo 113-0033, Japan
[6] Research Center for the Early Universe, University of Tokyo, Tokyo 113-0033, Japan
[7] Subaru Telescope, National Astronomical Observatory of Japan, 650 North Aohoku Place, Hilo, HI 96720, USA

Abstract

We present predictions for time delays between multiple images of the gravitationally lensed supernova, iPTF16geu, which was recently discovered from the intermediate Palomar Transient Factory (iPTF). As the supernova is of Type Ia where the intrinsic luminosity is usually well known, accurately measured time delays of the multiple images could provide tight constraints on the Hubble constant. According to our lens mass models constrained by the *Hubble Space Telescope* F814W image, we expect the maximum relative time delay to be less than a day, which is consistent with the maximum of 100 hr reported by Goobar et al. but places a stringent upper limit. Furthermore, the fluxes of most of the supernova images depart from expected values suggesting that they are affected by microlensing. The microlensing timescales are small enough that they may pose significant problems to measure the time delays reliably. Our lensing rate calculation indicates that the occurrence of a lensed SN in iPTF is likely. However, the observed total magnification of iPTF16geu is larger than expected, given its redshift. This may be a further indication of ongoing microlensing in this system.

Key words: gravitational lensing: strong – supernovae: individual (iPTF16geu)

1. Introduction

Occurrence of strongly lensed supernovae (SNe) has long been predicted (Refsdal 1964; Goobar et al. 2002b; Oguri et al. 2003; Oguri & Marshall 2010), but they had not been discovered until very recently. Quimby et al. (2013, 2014) reported the discovery of a strongly lensed Type Ia supernova (SN Ia) PS1-10afx with a total magnification of $\mu \sim 30$, although multiple images were not resolved. First resolved multiple images of a lensed SN were reported by Kelly et al. (2015): SN Refsdal, a core-collapse SN, that is strongly lensed into multiple images by a foreground galaxy cluster.

Although many strongly lensed galaxies and quasars have already been discovered, strongly lensed SNe have notable advantages over traditional strong lenses, particularly if they are of Type Ia. This is because of the standard candle nature of SNe Ia, which allows us to measure the magnification factor directly. While measurements of the Hubble constant from time delays (e.g., Suyu et al. 2014; Bonvin et al. 2016; Wong et al. 2016) need to overcome various degeneracies including the mass-sheet degeneracy (Falco et al. 1985; Schneider & Sluse 2014), the magnification factor provides important information on the lens potential, which directly breaks the mass-sheet degeneracy (Kolatt & Bartelmann 1998) and the degeneracy in the lens potential and the Hubble constant from time-delay measurements (Oguri & Kawano 2003). Indeed, several lensed SNe Ia behind massive clusters, although not multiply imaged, have been used to constrain mass distributions of foreground clusters (Riehm et al. 2011; Patel et al. 2014; Rodney et al. 2015).

Recently, Goobar et al. (2016, hereafter, G16) reported the discovery of a new gravitationally lensed SN Ia iPTF16geu

from intermediate Palomar Transient Factory (iPTF). In this Letter, we present time-delay predictions and interpret SN magnifications in light of microlensing. This Letter is organized as follows. We introduce iPTF16geu in Section 2 and describe our mass modeling method in Section 3. We present predictions for magnifications and time delays and discuss the role of microlensing in Section 4. We calculate the expected frequency of lensed SNe Ia in Section 5 and give our conclusions in Section 6.

2. iPTF16geu

The SN Ia of iPTF16geu has a redshift $z_{SN} = 0.409$ and is magnified by a factor of $\mu \sim 56$ by an intervening galaxy at $z_l = 0.216$ (G16). After spectroscopic confirmation, several follow-up programs were triggered to resolve the multiple images and measure light curves and time delays. Among the ground-based follow-up, data taken with OSIRIS on Keck with adaptive optics on 2016 October 13 yielded an image quality with FWHM = $0''07$ in the *H* band, establishing the presence of multiple lensed images of the SN. However, only two brighter SN images were visible because light from the host galaxy dominated the emission at near-infrared (NIR) wavelengths. Subsequent high-resolution images taken by the *Hubble Space Telescope* (*HST*) in the optical clearly revealed four SN images (DD 14862, PI: Goobar). In this Letter, we use the *HST* image taken on 2016 October 28 since it is deeper than images taken at previous epochs. We choose the F814W band which shows all SN images clearly (labeled A–D in descending order of their fluxes; see Figure 1).
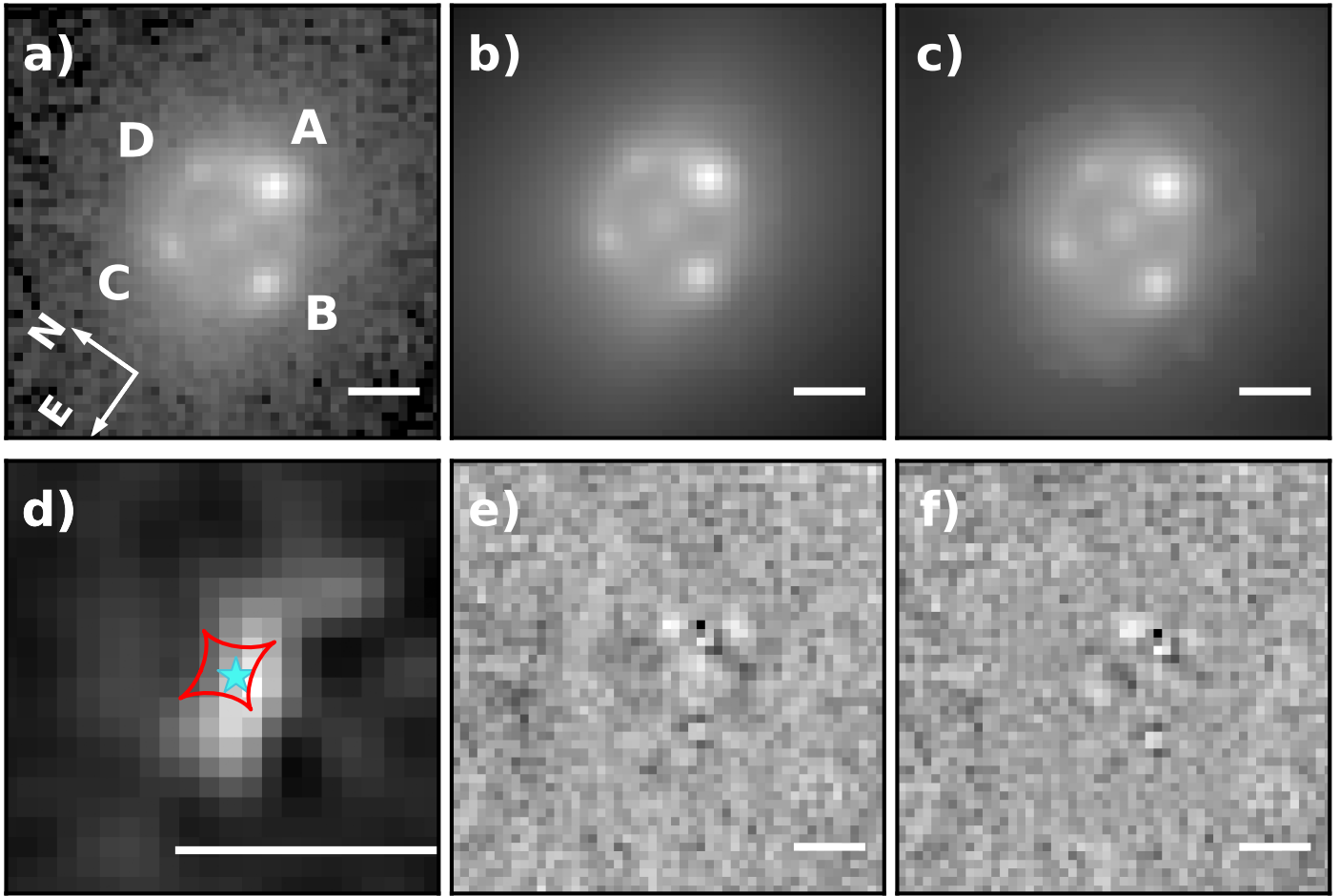
Figure 1. (a) *HST* image (F814W) of iPTF16geu (2016 October 28). Lens mass models from (b) GLAFIC and (c) GLEE and normalized residual images (e) and (f) in the bottom row, respectively. (d) The reconstructed surface brightness distribution of the SN host galaxy from the most-probable lens model of GLEE. Caustics (red curves) and the location of SN (blue star) are also shown. Images are $2''$ on the side, except for panel (d) which is $0''.5$ and all scale bars correspond to $0''.3$.

3. Lens Mass Modeling

We model iPTF16geu with two different mass modeling software: GLAFIC (Oguri 2010) and GLEE (Suyu & Halkola 2010; Suyu et al. 2012). This work is done independently by different coauthors, providing cross validation of our model results and predictions. Our cosmology is set to $\Omega_m = 0.32$, $\Omega_\Lambda = 0.68$, and $h = 0.72$. The corresponding time-delay distance for the lens system is $D_{\Delta t} = 1920$ Mpc.

The four SN images in iPTF16geu are almost equidistant from each other in a cross-like configuration where we expect the multiple images to be magnified by similar factors unlike what we see in iPTF16geu. Since the fluxes can be affected due to effects such as microlensing and time delay, we model each supernova image as a point-spread function with a free amplitude in the image plane. Additional data constraints come from the extended host galaxy, which is lensed into almost an Einstein ring. Both the software model the light of foreground lens galaxy with a Sérsic profile (Sérsic 1968), but differ in their assumptions about the mass profile of the lens and the model for the SN host galaxy.

3.1. Parametric Source Model

We fit the arbitrary SN fluxes simultaneously as we fit the SN positions and the lensed host (Sérsic) with lens mass model using GLAFIC. The lens mass distribution is modeled as a singular isothermal ellipsoid (SIE). We imposed the following constraints on the lens parameters. The centroid, axis ratio (q_m), and position angle (PA, φ_e) are assumed to be the same for the mass density and light profiles. External shear (γ_{ext}) is often degenerate with the ellipticity of the mass distribution. Hence, we did not include any external shear and were able to find a good model fit (see the middle column in Figure 1). We used a custom EMCEE (Foreman-Mackey et al. 2013) wrapper around GLAFIC to sample the posterior distribution of our models using the Markov Chain Monte Carlo (MCMC) approach.

3.2. Pixelated Source Model

With GLEE, we fit the SN images on the image plane simultaneously with its host galaxy surface brightness that is modeled on a grid of pixels on the source plane (Suyu et al. 2006). We use a power-law mass distribution for the lensing galaxy (e.g., Barkana 1998), with six parameters: centroid (θ_{m1}, θ_{m2}), q_m, φ_e, Einstein radius θ_E and radial mass profile slope γ' corresponding to the three-dimensional mass density $\rho \propto r^{-\gamma'}$. We also test SIE model for comparison with results of GLAFIC. We further consider a lens model that includes an external shear component, with the shear magnitude (γ_{ext}) and angle (φ_{ext}) as two additional parameters. The lensed arcs of the SN host galaxy and the fitted SN image positions provide constraints on the lens mass parameters. The SN and lens mass/light parameters have uniform priors. We

Table 1
Model Parameters and Predictions

Model Profile	Lens Model					κ, γ			
	$\theta_E('')$	q_m	φ_e	γ'	$\gamma_{ext}, \varphi_{ext}$	A	B	C	D
GLAFIC SIE	0.29 ± 0.01	0.83 ± 0.01	65 ± 1	$\equiv 2.0$	...	0.56, 0.56	0.43, 0.43	0.57, 0.56	0.46, 0.45
GLEE SIE	0.294 ± 0.002	$0.77^{+0.03}_{-0.02}$	66 ± 1	$\equiv 2.0$	...	0.60, 0.60	0.40, 0.40	0.62, 0.62	0.43, 0.43
GLEE PL	0.30 ± 0.01	0.73 ± 0.04	66 ± 1	2.1 ± 0.1	...	0.56, 0.66	0.35, 0.44	0.58, 0.68	0.38, 0.48
GLEE PL+γ_{ext}	0.30 ± 0.01	$0.66^{+0.08}_{-0.04}$	68^{+4}_{-2}	2.1 ± 0.1	$0.02^{+0.03}_{-0.01}, 79^{+8}_{-14}$	0.63, 0.61	0.36, 0.44	0.64, 0.64	0.40, 0.47

Model Predictions

Model Profile	Magnification Factors				Δt (days)			
	A	B	C	D	A	B	C	D
GLAFIC SIE	$-8.2^{+0.4}_{-0.5}$	$7.2^{+0.2}_{-0.2}$	$-7.1^{+0.3}_{-0.3}$	$10.8^{+0.4}_{-0.4}$	$0.40^{+0.02}_{-0.02}$	$\equiv 0$	$0.47^{+0.01}_{-0.02}$	$0.25^{+0.01}_{-0.01}$
GLEE SIE	$-6.7^{+1.2}_{-1.0}$	$5.6^{+0.6}_{-0.6}$	$-4.5^{+0.6}_{-0.6}$	$8.7^{+1.1}_{-1.3}$	$0.52^{+0.08}_{-0.05}$	$\equiv 0$	$0.65^{+0.07}_{-0.07}$	$0.35^{+0.05}_{-0.05}$
GLEE PL	$-5.5^{+0.9}_{-1.5}$	$4.8^{+0.9}_{-0.6}$	$-3.7^{+0.5}_{-0.9}$	$7.4^{+1.6}_{-0.9}$	$0.56^{+0.06}_{-0.06}$	$\equiv 0$	$0.70^{+0.06}_{-0.07}$	$0.37^{+0.03}_{-0.04}$
GLEE PL+γ_{ext}	$-5.2^{+1.7}_{-1.9}$	$4.7^{+1.3}_{-1.2}$	$-3.6^{+1.2}_{-1.3}$	$7.4^{+1.9}_{-2.0}$	0.6 ± 0.1	$\equiv 0$	0.7 ± 0.1	0.4 ± 0.1

Note. θ_E is the Einstein radius. q_m is the axis ratio of the lens mass. The PAs (φ_e and φ_{ext}) are in degrees measured east of north. A shear angle of $\varphi_{ext} = 0$ corresponds to shearing of the lens system along the north–south direction. The most-probable convergence (κ) and shear (γ) values are given at the location of each SN image. Negative magnification (μ) means opposite parity and Δt is time delay relative to image B.

sample all the model parameters using either EMCEE or the MCMC method described in Dunkley et al. (2005).

4. Results and Discussion

In Figure 1, we show images of our most-probable models (top row—panels (b) and (c)) and the corresponding residuals (model subtracted from the data, normalized by the estimated pixel uncertainties; bottom row—panels (e) and (f)). The pixelated reconstruction of the SN host galaxy on the source plane from GLEE is also shown (panel (d)) with the location of the SN (star). Parts of the host galaxy and the SN lie within the astroid caustic (red curve) and are thus quadruply imaged, whereas other parts are doubly imaged.

We also present our modeling results from both GLAFIC and GLEE in Table 1 and they agree reasonably well. The median of the posterior distributions and their 68% confidence levels for the lens parameters are given. The slope of the density profile is consistent with isothermal ($\gamma' = 2.0$) within the uncertainties. The power-law models with and without γ_{ext} are the same within the uncertainties suggesting that the role of γ_{ext} is not significant. We give the convergence (κ), which is the surface mass density in the units of critical surface mass density and shear values at the location of SN images A, B, C, and D in Table 1. We also give predictions for magnifications and relative time delays. Negative magnifications imply opposite parity of the images and that they correspond to saddle points in the time-delay surface (e.g., Blandford & Narayan 1986). As expected, the predicted relative magnifications are comparable (within a factor of 2) for all SN images. Light from image B arrives first, followed by images D, A and C consistently for all our models. Images A and C are saddle images (negative parity) and images B and D are minima (positive parity). We find that the time delays (relative to image B) are within a day, a more stringent limit than the 100 hr range predicted by G16.

Now, we use the standard candle nature of SN Ia to our advantage in understanding expected and observed SN fluxes. We take the best-fit Sloan Digital Sky Survey (SDSS) i-band model light curve from G16 (corresponding to F814W). After accounting for time dilation and dust extinction of $E(B - V) = 0.31$ assuming $Rv = 3.1$, we calculate the unlensed SN flux expected on 2016 October 28 (35 days from maximum) to be 24.21 ABmag. In Figure 2, we show the unlensed SN flux scaled up by magnification factors from our models (filled symbols). For comparison, we also plot the observed PSF fluxes of the SN images (open symbols, based on fits by the two modeling software). It is interesting to note that image D, which appears the faintest in the data, is predicted to have the largest magnification factor. Image C is the least magnified of all and most consistent with expected magnification. Both images A and B are expected to be fainter than D in the absence of any external factors affecting the fluxes, but are found to be greatly magnified.

Since the relative time delays are less than a day from our models, differences in the observed fluxes are unlikely to be due to time delays. While differential dust extinction could be a possible cause of anomalies in fluxes, it is unlikely to produce such large differences, given the almost symmetrical distribution of SN images around the lens, which is an early-type galaxy (e.g., Falco et al. 1999; Elíasdóttir et al. 2006, also, G16 suggest that extinction is not significant). The most likely explanation for highly anomalous fluxes is microlensing due to stars in the foreground lens galaxy.[8]

Saddle images are more susceptible to show microlensing (de-)magnification in their fluxes, whereas minimum images typically have enhanced fluxes over the macro-magnification (i.e., magnification from a smooth mass model; e.g., Kochanek 2006). Indeed, we find that image A, located at a saddle point, is brighter than our smooth mass model predictions by nearly two magnitudes for the epoch presented here. Images B and D, which are at minima, are found to be magnified and suppressed, respectively, by nearly a magnitude each. Image C does not seem to be affected by microlensing. However, we need to analyze multi-epoch data in order to be certain about the extent

[8] We do not consider lensing by subhalo or millilensing explicitly because it essentially has the same consequences qualitatively as microlensing in single epoch images, but arising due to a more massive subhalo instead of stars. With superior resolution and multi-epoch data, it may be possible to disentangle between millilensing (static) and microlensing (time-varying) effects. We restrict our discussion to microlensing for iPTF16geu which we believe has a higher optical depth, but we acknowledge the possible presence of millilensing.
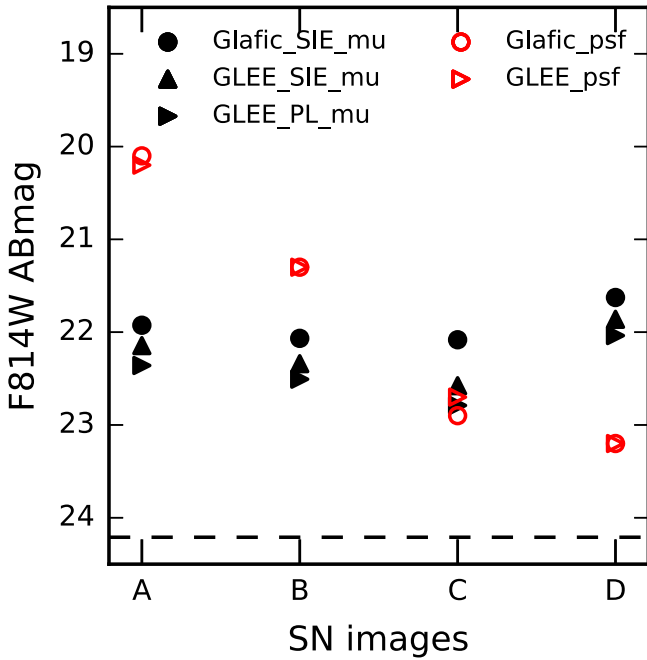
Figure 2. Fluxes of SN images A, B, C, and D. Expected fluxes after scaling the intrinsic SN flux (24.21 ABmag, dashed line) by the lens-model magnification (μ) factors (filled symbols) are compared with PSF model fluxes fit to the *HST* image. Relative magnifications are more robust than the absolute values across different models. Fluxes of most of the images depart from predictions. Image A is the most magnified and image D appears to be suppressed (see Section 4 for further discussion).
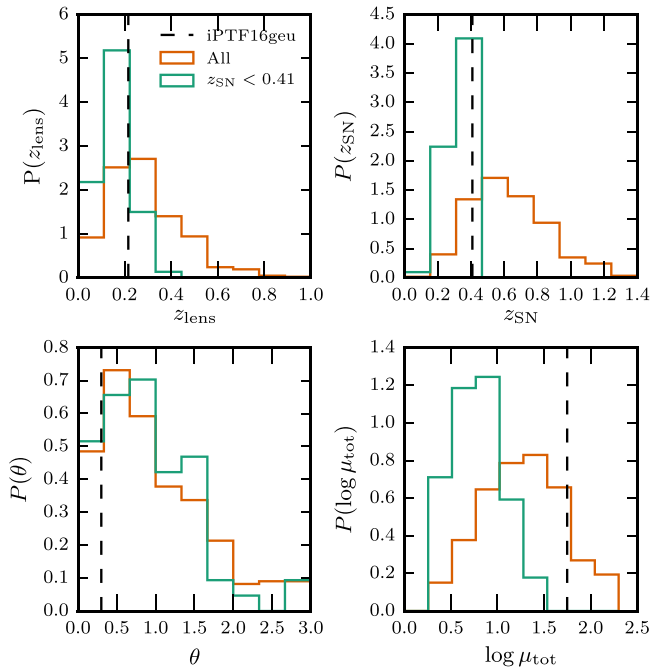
Figure 3. Expected distributions of the lens redshift z_l (upper left), source (SN), redshift z_{SN} (upper right), image separation θ (lower left), and total magnification μ_{tot} (lower right), in iPTF and PTF, which are computed using the method described in Oguri & Marshall (2010) with some modifications to match the selection function of PTF/iPTF.

to which each of the images are affected by microlensing. This work is left to a future paper.

Dobler & Keeton (2006) calculated the optical depths for microlensing of lensed SN Ia and found a high probability for

lensed SNe to be affected by microlensing. Using typical stellar mass fractions measured from the lens galaxies of the Sloan ACS Survey (Bolton et al. 2004), they found that 25% of lensed SN Ia showed differences of more than 1 magnitude. The stellar mass fraction ($< \theta_E$) for the lens in iPTF16geu is ~ 0.9 derived using stellar mass—velocity dispersion ($M_* - \sigma$) relation (Zahid et al. 2016 and references therein). This suggests a high optical depth, although there is a large uncertainty in the mass fraction due to the scatter (about a factor of 2) in the $M_* - \sigma$ relation. For a typical SN photosphere size (10^{15} cm) and lens velocity dispersion (~ 150 km s^{-1}), we calculate caustic crossing time to be ~ 2 years (e.g., Treyer & Wambsganss 2004). On the other hand, SN photosphere velocities of 15,000 km s^{-1} imply that microlensing effects could be visible on shorter timescales corresponding to the light curve. Microlensing can affect SN Ia light curves on different timescales and produce different qualitative signatures (e.g., large magnitude offsets, introduce non-intrinsic peaks, change the decay rate), thus making it difficult to measure time delays with accuracy better than a few days (Dobler & Keeton 2006).

5. Frequency of Lensed SN Ia

G16 used the SNOC Monte Carlo package (Goobar et al. 2002a) to calculate the expected number of lensed SNe Ia with high magnification and found that it appears to be too low to explain the discovery of iPTF16geu. Based on this comparison, they argued that lensing by sub-kiloparsec structures may have been greatly underestimated. Here, we present an independent comparison of the expected number and property of strongly lensed SN Ia with iPTF16geu.

Our estimate of the expected lensing rate is based on Monte Carlo simulations presented in Oguri & Marshall (2010), in which realistic population of lensing galaxies and the source population has been considered, and various selection biases such as magnification bias and K-correction have been properly taken into account. Mass distributions of lensing galaxies are assumed to follow the SIE with an external shear. Here, the velocity function of galaxies of all types directly measured in SDSS (Bernardi et al. 2010) is used for the abundance of lensing galaxies. However, calculations of Oguri & Marshall (2010) assumed that multiple images be resolved in surveys, which was not the case for iPTF. The poor spatial resolution of iPTF makes most of multiply imaged SNe blended. In order to compute lensing rates in such a situation, we use the total magnification, rather than magnifications of individual images used in Oguri & Marshall (2010), to compute the magnification bias. We also impose no lower limit on the image separation (see also Quimby et al. 2014).

In order to compute the expected total number of lensed SNe Ia, we need to know the total survey volume of iPTF. According to G16, the total monitoring time and the average solid angle of iPTF and PTF (precursor survey to iPTF) translates into the total survey volume of ~ 5000 deg^2 years, which we adopt in the following calculations. The detection limit is $R \sim 21$, but in order to observe light curves well we assume that peak magnitudes of SNe be one magnitude brighter than the limiting magnitude in order to be detected and studied in iPTF, i.e., the limiting magnitude of the peak SN brightness of $R = 20$.

We find that the expected number of lensed SNe Ia in iPTF and PTF calculated using the setup above is 0.9, which would be consistent with the discovery of iPTF16geu. The probability

distribution for the expected redshifts, image separation, and magnifications are shown using orange histograms and compared to iPTF16geu (vertical dashed line) in Figure 3. Because of the large effect of the magnification bias, our calculation also predicts a high fraction of quadruple lenses, ∼65%, which is consistent with iPTF16geu being a quadruple lens. However, the efficiency of the spectroscopic typing of iPTF events goes down at $z \gtrsim 0.41$ (A. Goobar 2016, private communication). The expected number of lensed SNe Ia with $z_{SN} < 0.41$ is 0.16 (see green histograms for distribution of properties), making it less likely to be discovered. The observed magnification of iPTF16geu in this case also appears inconsistent given the distribution. This is in agreement with G16, who require extreme assumptions about the fraction of compact objects in halos. This may be further evidence for the presence of microlensing.

6. Conclusion

We have presented lens modeling results for the recently discovered gravitationally lensed SN Ia, iPTF16geu (G16). Our mass modeling predicts flux ratios within a factor of 2 across the four lensed images of the SN. However, the brightest images A and B are nearly 15 and 5 times brighter, respectively, than the fainter pair of images (C and D) as measured from the *HST* F814W image. Differential extinction may have very little to no contribution, as noted in G16, especially at NIR. And, yet the high contrast in flux ratios appears similar at other optical and NIR wavelengths (see G16).

Our interpretation is that most of the SN images are affected by microlensing. We derived the unlensed SN flux for the epoch of October 28 using the best-fit model light curve (G16). Multiplying the unlensed SN flux by our lens-model magnification factors suggests that, in addition to the macro-magnification, fluxes of images A and B are further magnified by more than a magnitude and image D is suppressed by nearly a magnitude due to microlensing. While image C does not seem to be affected by microlensing from the current analysis, we need to analyze multi-epoch data to understand how each of the SN images are affected by microlensing.

We predict relative time delays of the order of less than a day, a consistent but more stringent upper limit than the hundred hours predicted in G16. Accurate measurements of the time delays will require observations with high cadence (∼a few hours apart) and preferably around characteristic features in the light curves. However, small time delays predicted in our mass modeling and probable microlensing effects suggest that accurate measurements of time delays may be quite challenging (e.g., Dobler & Keeton 2006).

Finally, based on our detailed calculations of lensing rates, the expected average number of lensed SN Ia from PTF/iPTF is 0.9. However the spectroscopic follow-up and typing efficiency implies a restriction of $z_{SN} < 0.41$ (G16; A. Goobar 2016, private communication), which reduces this expected number to 0.16. This also implies that the high observed magnification of iPTF16geu is quite unlikely, and hints at a possible role of microlensing.

Facility: HST(WFC3).

References

Barkana, R. 1998, ApJ, 502, 531
Bernardi, M., Shankar, F., Hyde, J. B., et al. 2010, MNRAS, 404, 2087
Blandford, R., & Narayan, R. 1986, ApJ, 310, 568
Bolton, A. S., Burles, S., Schlegel, D. J., Eisenstein, D. J., & Brinkmann, J. 2004, AJ, 127, 1860
Bonvin, V., Courbin, F., Suyu, S. H., et al. 2016, arXiv:1607.01790
Dobler, G., & Keeton, C. R. 2006, ApJ, 653, 1391
Dunkley, J., Bucher, M., Ferreira, P. G., Moodley, K., & Skordis, C. 2005, MNRAS, 356, 925
Elíasdóttir, Á., Hjorth, J., Toft, S., Burud, I., & Paraficz, D. 2006, ApJS, 166, 443
Falco, E. E., Gorenstein, M. V., & Shapiro, I. I. 1985, ApJL, 289, L1
Falco, E. E., Impey, C. D., Kochanek, C. S., et al. 1999, ApJ, 523, 617
Foreman-Mackey, D., Hogg, D. W., Lang, D., & Goodman, J. 2013, PASP, 125, 306
Goobar, A., Amanullah, R., Kulkarni, S. R., et al. 2016, arXiv:1611.00014
Goobar, A., Mörtsell, E., Amanullah, R., et al. 2002a, A&A, 392, 757
Goobar, A., Mörtsell, E., Amanullah, R., & Nugent, P. 2002b, A&A, 393, 25
Kelly, P. L., Rodney, S. A., Treu, T., et al. 2015, Sci, 347, 1123
Kochanek, C. S. 2006, in Proc. Saas-Fee Advanced Course 33 Conf., Gravitational Lensing: Strong, Weak and Micro, ed. G. Meylan, P. Jetzer, & P. North (Berlin: Springer), 91
Kolatt, T. S., & Bartelmann, M. 1998, MNRAS, 296, 763
Oguri, M. 2010, PASJ, 62, 1017
Oguri, M., & Kawano, Y. 2003, MNRAS, 338, L25
Oguri, M., & Marshall, P. J. 2010, MNRAS, 405, 2579
Oguri, M., Suto, Y., & Turner, E. L. 2003, ApJ, 583, 584
Patel, B., McCully, C., Jha, S. W., et al. 2014, ApJ, 786, 9
Quimby, R. M., Oguri, M., More, A., et al. 2014, Sci, 344, 396
Quimby, R. M., Werner, M. C., Oguri, M., et al. 2013, ApJL, 768, L20
Refsdal, S. 1964, MNRAS, 128, 307
Riehm, T., Mörtsell, E., Goobar, A., et al. 2011, A&A, 536, A94
Rodney, S. A., Patel, B., Scolnic, D., et al. 2015, ApJ, 811, 70
Schneider, P., & Sluse, D. 2014, A&A, 564, A103
Sérsic, J. L. 1968, Atlas de Galaxias Australes (Cordoba: Observatorio Astronomico)
Suyu, S. H., & Halkola, A. 2010, A&A, 524, A94
Suyu, S. H., Marshall, P. J., Hobson, M. P., & Blandford, R. D. 2006, MNRAS, 371, 983
Suyu, S. H., Hensel, S. W., McKean, J. P., et al. 2012, ApJ, 750, 10
Suyu, S. H., Treu, T., Hilbert, S., et al. 2014, ApJL, 788, L35
Treyer, M., & Wambsganss, J. 2004, A&A, 416, 19
Wong, K. C., Suyu, S. H., Auger, M. W., et al. 2016, arXiv:1607.01403
Zahid, H. J., Geller, M. J., Fabricant, D. G., & Hwang, H. S. 2016, ApJ, 832, 203